P-Delays from Floating Seismometers (MERMAID), Part I: Data Processing

by Cécile Joubert, Guust Nolet, Sébastien Bonnieux, Anne Deschamps, Jean-Xavier Dessa, and Yann Hello

ABSTRACT

We present methods of data analysis adapted to Mobile Earthquake Recorder in Marine Areas by Independent Divers (MERMAID) seismograms, obtained with hydrophones mounted on moving underwater floats. If the MERMAID float comes immediately to the surface after recording an earthquake signal, the seismogram location is obtained from the first Global Positioning System (GPS) position, using a correction for the surface drift of the float. In the case of earthquakes recorded without an immediate surfacing, the location is estimated using a linear interpolation between GPS positions. We performed a Bézier interpolation of the GPS positions to estimate a location error. In 67% of the cases, the distance between the two trajectories was less than 500 m. We tested the method on six months of data acquired in the Ligurian basin (Mediterranean Sea). To validate the (manually) picked onset times for *P* waves, we performed a preliminary tomographic inversion beneath the Ligurian basin of MERMAID data together with a much larger volume of picks from nearby land and ocean-bottom seismometer stations. After inversion we found that 67% of MERMAID data have a misfit between ± 0.17 s, but the distribution of misfits is not Gaussian and shows outliers. We conclude that floating seismometers are an excellent and accurate means for covering oceanic areas for *P*-wave tomography.

INTRODUCTION

The global tomography image of the Earth's southern hemisphere is poorly constrained because of the predominance of oceanic domains, which does not allow us to deploy many seismic stations (Hello *et al.*, 2011). To overcome this difficulty Simons *et al.* (2006) proposed to record *P* waves in the oceans with a hydrophone mounted on a drifting float, known as a Mobile Earthquake Recorder in Marine Areas by Independent Divers (MERMAID).

MERMAID floats belong to the Lagrangian floats family, such as routinely used in the global oceanographic Array for Realtime Geostrophic Oceanography (ARGO) project (Dalton, 2002; Gould, 2004). However, a typical dive of a MERMAID float differs from that of an ARGO float. There are three main steps:

- At the beginning of a cycle, the float downloads new instructions (if these have been sent), and the float dives to the desired parking depth.
- At the parking depth, the float records signals with a low-frequency hydrophone (Rafos II). When a high-amplitude signal is recorded, an onboard analysis is performed to identify the signal type with a discrimination software based on the wavelet transform (Sukhovich *et al.*, 2011). If the recorded signal corresponds to a *P* wave, two scenarios are possible:
  a. If the likelihood that the wave is a *P* wave exceeds a (programmable) threshold, the float rises to the surface and transmits all data, including stored seismograms from earlier triggers, from the buffer to the satellite. Only the stored signals with the ten highest probabilities are transmitted, so little energy is lost on transmission of false triggers.
  b. If the probability is not high enough, the float stores the recorded signal in the memory card for a transmission when a stronger signal arrives or when a specified period is exceeded (usually 10 days). This is done to conserve energy.
- The float dives, and another cycle begins.

During surfacing, the two-way communication allows us to change depth, filtering, and discrimination parameters. For the experiment reported in the article, we used three MERMAID floats. Currently, four other MERMAIDs are deployed in the Indian Ocean and nine in the Pacific Ocean. Data from the Mediterranean Sea and Indian Ocean are available from Géoazur laboratory (currently at https://geoazur.fr/GLOBALSEIS/Data.html, last accessed November 2015).

There are many sources of errors that are not encountered in land-based stations: the ocean environment has high microseismic noise in addition to noise from ships, mammals, and other sources. The uncertainty in the precise recording location is another new source of error. To estimate typical delay time errors, we performed a tomographic study to evaluate MERMAID data consistency with other seismological data from terrestrial and fixed marine stations (Fig. 1). The Ligurian Sea, in the central Mediterranean Sea, with ocean-bottom seismometer (OBS) deployments and nearby land stations easily available, presents an ideal location for such a test.

doi: 10.1785/0220150111

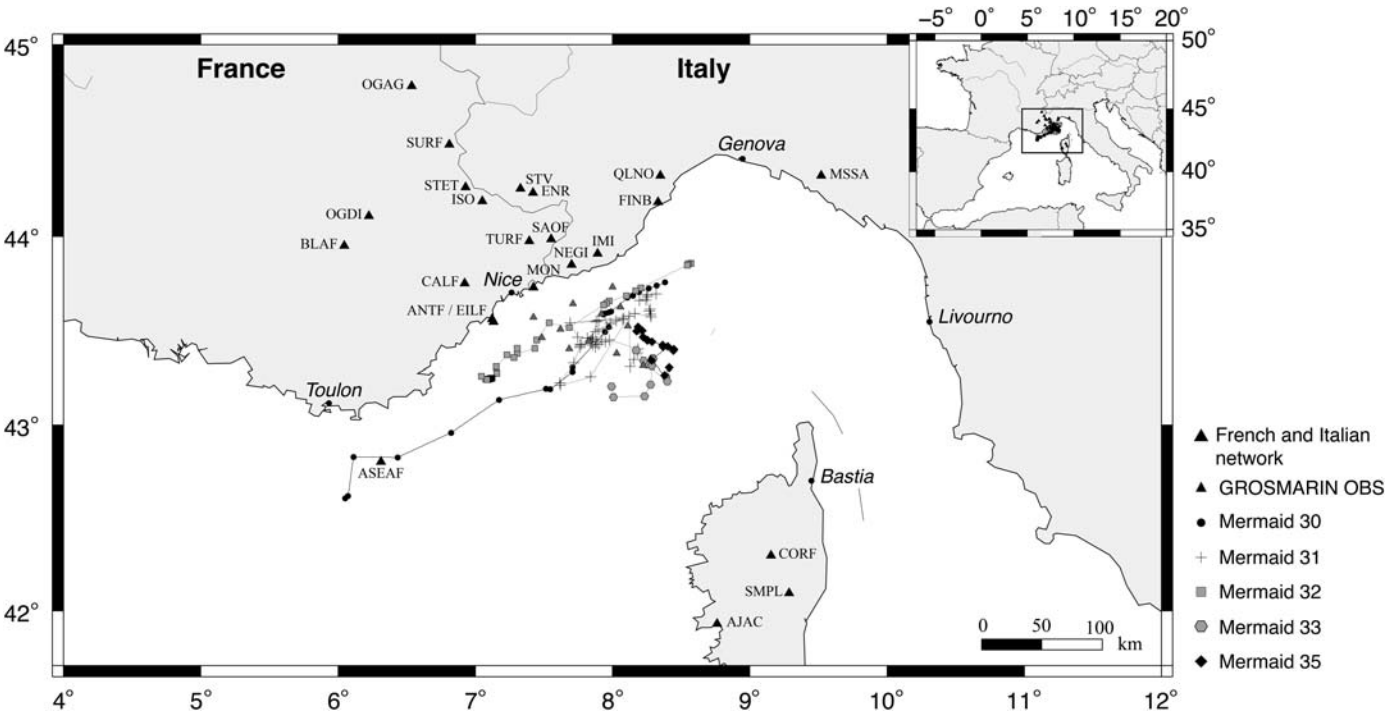

▲ **Figure 1.** Study zone and associated locations of stations used in this study. Terrestrial permanent stations in France and Italy are symbolized by large black triangles. The ocean-bottom seismometers (OBSs) used in the Grand Réseaux d'Observations Sous-MARIN (GROSMARIN) campaign are in small black triangles. Mobile Earthquake Recorder in Marine Areas by Independent Divers (MERMAID) float trajectories are indicated by different symbols for each float (MERMAID 33 and 35 correspond to MERMAID 30 and 32 redeployments).

The MERMAIDs have no fixed location and can serve as a low-cost addition to interpolate *P*-wave delays between permanent locations, thus increasing the resolution of tomographic studies. MERMAIDs constitute an option for seismic monitoring that is complementary to that of using cabled instruments such as in the Cascadia experiment (Gao and Schwartz, 2015).

MERMAID DATA PREPROCESSING STAGES

We present here the preprocessing stages required for the incorporation of the new kind of data in a tomographic inversion using manual *P*-phase picking.

We need to correct the first transmitted Global Positioning System (GPS) position for the drift until the connection is established with a satellite to obtain the position of the float at the time of recording. The positions for seismometers for earthquakes that have not triggered an automatic ascent of the float require interpolation between two GPS positions.

MERMAID Float Surface-Drift Correction

When the float reaches the surface, it may take between 5 and 30 min to establish a GPS position. During this time gap, the float drifts at the surface, and we have to take this into account. The Ligurian Sea is subjected to a strong current, the Ligurian current (Béthoux *et al.*, 1988). In our experiment, we observed a mean surface drift of 0.27 m/s and a maximum of 0.79 m/s (Fig. 2).

When the float reaches the surface, the surfacing time is stored in the float log. While the satellite is connected, several GPS positions are transmitted. The first two GPS positions are used to perform a linear extrapolation of the float trajectory at the surface, to determine the float position at the time it came to the surface.

This correction does not yet take into account the potential horizontal drift of the float during its vertical ascent. We lack information to correct for it and assume that the location of the float is the same at depth and when arriving at the surface. A seismic swarm, which occurred at the Indian Ocean triple junction point (23–24 October 2013), allowed us to study this horizontal drift. The swarm led to several successive cycles of ascent and descent of the floats, and the positions at surfacing were close (Sukhovich *et al.*, 2015), which gave an upper limit of 500 m for the error introduced by this assumption, though the more typical error is estimated to be less than half of that. As we discuss later (Fig. 5), such mislocations led to an equivalent error in delay times of < 0.1 s.

MERMAID Water-Depth Correction

The MERMAID float (based on an Autonomous Profiling EXplorer [APEX] float, design from Teledyne Webb Research) can be deployed to 1732 m depth (this limitation is in particular due to the hydrophone depth resistance). A typical depth of 1500 m is used. Unlike OBS instruments, MERMAID floats drift above the seafloor. When an earthquake is recorded, in order to interpret the arrival time at the seafloor, we shall wish to reduce all arrival times to the arrival time at the seafloor (as used for an OBS) and must correct for the time needed by the *P* wave to travel from

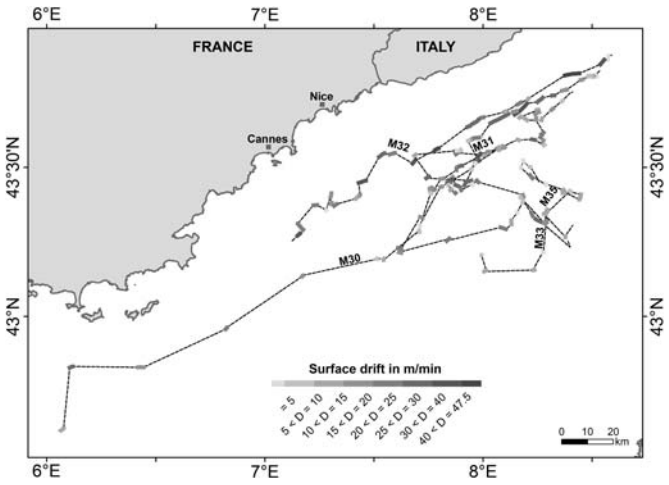

▲ **Figure 2.** The trajectories of floats used in the experiment are shown. Thick lines indicated surface drift (in meters per minute) with velocity in grayscale. MERMAID floats are labeled M30–M33 and M35.

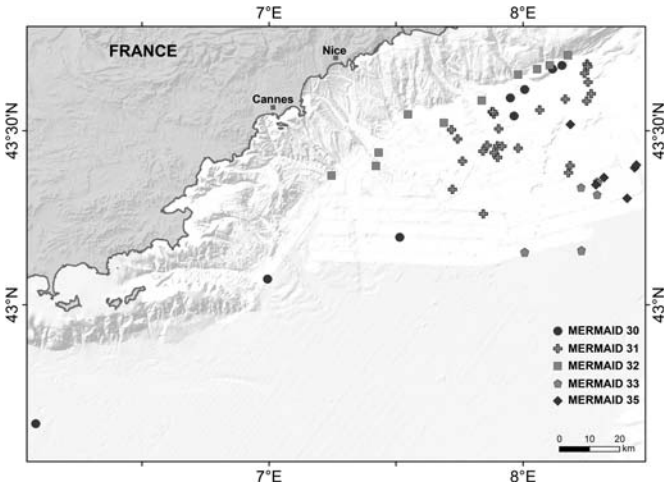

▲ **Figure 3.** Floats positions during earthquakes recording. Symbols correspond to associated MERMAID floats positions.

the seafloor to the MERMAID float. To do this, we used a very precise bathymetric synthesis with 25 m lateral resolution from the MArge LIgure par utilisation du Système Acoustique Remorqué (MALISAR) oceanographic campaigns performed in the zone (Migeon *et al.*, 2011). The minimum lateral resolution of the bathymetric map required is given by the Fresnel zone. Considering that the MERMAID float is drifting at a distance z from the seafloor, we can estimate the Fresnel zone diameter D (defined by the diffracted wave being $\pi/2$ out of phase with the direct arrival) from equation (1), in which λ corresponds to the wavelength:

$$D = \sqrt{2z\lambda + \frac{\lambda^2}{4}}. \quad (1)$$

In our case, the floats were immersed near 1500 m depth, and the mean bathymetry of the seafloor was around 2200 m ($z = 700$ m); considering a frequency of $f = 1$ Hz and $\lambda = 1500$ m, we obtain a minimum lateral resolution required of the bathymetric map of $D = 1632$ m, which is respected in our study with a lateral resolution of 25 m.

Figure 3 illustrates the MERMAID float GPS positions at the times an earthquake was recorded. Only two GPS positions are outside this MALISAR bathymetry coverage, MERMAID 30 in the southwest of the Figure 3 and MERMAID 33 in the east of the Figure 3. In these two cases, the lateral resolution is about 100 m (using the International Bathymetric Chart of the Mediterranean [IBCM]).

To correct for the MERMAID depth, we use the fact that we have an almost vertical wave direction in the water and subtract a vertical travel time $z/1500$ (in which 1500 is the velocity in meters per second) from the picked time.

The seafloor depth is taken into account in the bathymetric correction. Variations in sediment thickness or deviations from CRUST2.0 (Bassin *et al.*, 2000) are not corrected for *a priori*, but are solved for in the inversion. If strong variations occur over distances longer than the voxel size (about 70 km), they add to the misfit.

Float Logs

At the end of a mission, the clock is synchronized by satellite and the clock drift is corrected. The precision of the clock is communicated as 1 μs/s. To observe a clock drift of 1 s, a mission of 10 days is necessary. All clocks are synchronized at least every 10 days if no significant earthquake had been recorded. Clock drift corrections are also recorded on the logs and usually correspond to a few milliseconds. All MERMAID float actions are recorded in the logs with their associated hours. In the preprocessing stage, a clock malfunction was detected for MERMAID 31. We observed an occasional clock jump of 1 s, from a course that is currently not identified, forcing us to momentarily reject all data from this float. This affects 30% of the MERMAID data obtained for this study.

Seismograms Recorded without Immediate Surfacing

When an earthquake is recorded and stored in memory without triggering a rise to the surface for immediate transmission, the record is sent to the satellite at the end of a dive cycle. In that particular case (open circles in Fig. 4), the position of the float is linearly interpolated from the last GPS position before the float dives and the first GPS position when it comes at the surface (symbolized by plain lines in Fig. 4a,b), assuming the drift velocity was constant. We observe that the drift at depth is different, and much slower, than the drift at the surface. The drift at depth is typically a few kilometers per day in the Ligurian and ~1.6 km/day in our experiment. Drift at the surface is influenced by the wind and may be an order of magnitude faster.

In our experiment, 30% of the data were recorded without immediate surfacing. To estimate the error in the linear approximation, we studied the undersea float drift. For this purpose, we seek the difference between linear and smoothly curved interpolated trajectories. For the latter, we use cubic Bézier interpolation through four points, which minimizes the undulations in the path (Bézier, 1977, 1987), shown as dashed lines in Figures 4a,b, following four main steps:

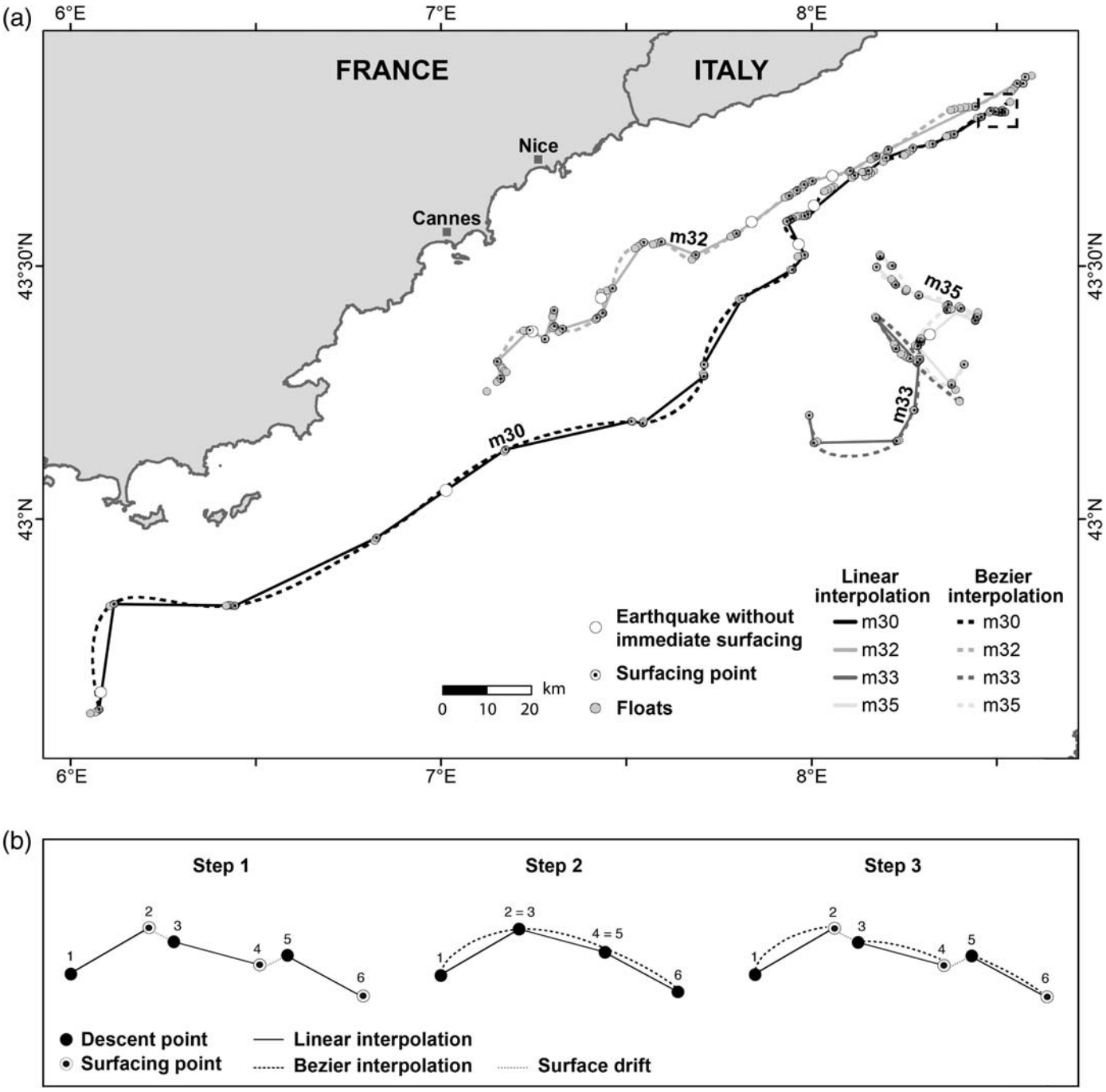

▲ **Figure 4.** (a) Bézier interpolation trajectories of MERMAID floats during an earthquake recording without an immediate surfacing (open circles). Linear trajectories of MERMAID floats are in solid curves and Bézier interpolations are in dotted curves. (b) Interpolations corresponding to the Bézier interpolation principle (see text).

- Because the surfacing offsets the deep trajectory with the surface drift (Figs. 1 and 2), we separate each segment of the float trajectory between each dive and surface points. We then translate surfacing point to coincide with the next dive point. For example, in Figure 4b the plain black segments correspond to the deep drift of the float. If we consider the cycle defined between two open circles: open circle 1 corresponds to the descent GPS position of the float and open circle 2 to the surfacing GPS position. At the end of the cycle, after the surface drift (gray dashed lines in Fig. 4b), the next cycle is then started at the descent GPS position 3, and the next surfacing position is shown by 4. To isolate the deep drift, we connect the ascent GPS position to the next descent position. In our example, it corresponds to a connection between open circles 2 and 3 and between 4 and 5. We do this along the whole trajectory of the MERMAID float.
- After the segments are juxtaposed, we perform a Bézier interpolation, symbolized by the dotted black curve in Figure 4b.

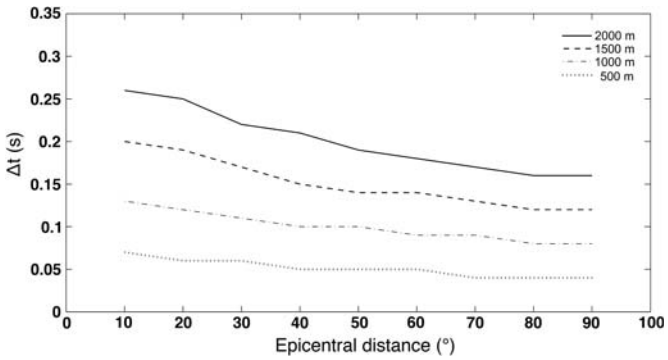

▲ **Figure 5.** Equivalent time errors (in seconds), as a function of the epicentral distance of an earthquake, in the case of a record without an immediate surfacing. The curves represent four typical locations errors (500, 1000, 1500, and 2000 m).

- For seismograms without an immediate surfacing, we use the obtained Bézier trajectory, replaced over the observed linear trajectory (Fig. 4b), to find a location that takes into account a possible curvature in the deep drift (Fig. 4a).
- We measure the distance between the Bézier and the linear by interpolated positions (Fig. 4b) and interpret this as an estimate of the typical error introduced by linear interpolation.

For the data without immediate surfacing, we observed a distribution of the distance Δd between the linear and Bézier interpolation trajectories in which 67% have $\Delta d \leq 500$ m, 0% with $500 < \Delta d \leq 1000$ m, 11% with $1000 < \Delta d \leq 1500$ m, 11% with $1500 < \Delta d \leq 2000$ m, and 11% with $\Delta d > 2100$ m. Even if the distance is large, it introduces a relatively small error in data. Figure 5 illustrates the equivalent delay time errors (Δt) observed for different distances, between the Bézier and linear trajectories, as a function of the angular distance. The larger the epicentral distance, the more horizontal the wavefront and, therefore, the smaller the time error. In the worst case observed in our experiment, for a Δd of 2090 m for an earthquake at an epicentral distance of 10°, we obtained an error of 0.27 s. We imposed a maximum authorized error of 0.3 s for data to be included in the tomographic interpretation discussed in the next section. About 67% of the interpolated data have an error < 0.1 s. The largest errors seem to occur where sharp gradients in coastal bathymetry cause the trajectory to bend, and such errors would be rare for floats drifting in the open ocean.

TOMOGRAPHIC TEST

Delay times δt observed between a source and a receiver, compared to a reference model, are caused by the velocities anomalies of the Earth but also are affected by errors in picking and in the corrections discussed in the preceding section. We do not exactly know the velocity anomalies inside the Earth, but we can test if the delay times observed in MERMAID data are consistent with terrestrial and OBS data (Fig. 1). To do so, we invert them simultaneously in a tomographic study.

We performed a tomographic inversion based on ray theory with manual picking phase of the *P*-wave arrival time and study of the delay times with respect to the reference model IASP91 (Kennett and Engdahl, 1991). We include correction of IASPEI times for the ellipticity of the Earth, as well as crustal corrections computed from the CRUST2.0 model (Bassin *et al.*, 2000). The important model we invert for is confined to a half-sphere with a radius of 600 km, beneath the Ligurian basin and the nearby continent. Of course our data are local and cannot resolve the global structure. The path outside of the direct volume of interest does influence the delays, though its effect is damped by the phenomenon of wavefront healing. We mimic this by including the rest of the Earth into the model, but subject to a higher damping than used for the structure beneath Liguria (see Bonnin *et al.*, 2014, for details). We used the voxel parameterization in a cubed Earth (Simons *et al.*, 2011; Charléty *et al.*, 2013), with cell sizes decreasing linearly from an average of 78 km at the surface to 43 km at the core–mantle boundary.

Dataset

To perform the tomographic inversion, we used different datasets from different kinds of instruments. All stations used are illustrated in Figure 1. *P*-wave onset times have been visually picked after removing noisy seismograms.

Terrestrial Permanent Stations of the French and Italian Networks

Figure 1 shows the locations of permanent stations in the French and Italian networks that were used in our study (large black triangles). We used seismograms of 17 French permanent stations, including three on Corsica. Earthquakes from 2004 until May 2014, with magnitudes between $6.5 \leq M_w \leq 7.5$ and epicentral distances between $0° \leq \Delta d \leq 90°$, were selected. Figure 6 illustrates two examples of seismograms recorded by terrestrial permanent stations. We used data from nine stations in northwest Italy. To allow for a balanced distribution of data, we used a somewhat lower threshold of $M_w \geq 6$ and epicentral distances between $0° \leq \Delta d \leq 90°$.

Grand Réseaux d'Observations Sous-MARIN Oceanographic Campaign

We used data from the Grand Réseaux d'Observations Sous-MARIN (GROSMARIN) oceanographic campaign that occurred from April to October in 2008 in the Ligurian basin (Dessa *et al.*, 2011). During this campaign, 21 OBS were deployed for two to five months (small black triangles in Fig. 1). We used local and teleseismic earthquakes with magnitudes higher than $M_w \geq 5$ and epicentral distance of $\Delta d \leq 105°$.

MERMAID Data

We incorporated six months of data from two MERMAID floats, each deployed twice near the northwest coast of Italy and drifting past the southeast of France (symbols in Fig. 1) between March and September of 2014. MERMAID 33 corresponds to MERMAID 30 redeployed. Figure 6 illustrates two examples of seismograms recorded by MERMAID floats for a regional event (Barcelonnette earthquake) and a teleseismic event (Hokkaïdo earthquake).

The final dataset contained 1127 delays from 199 earthquakes with global coverage illustrated in Figure 7. Data from

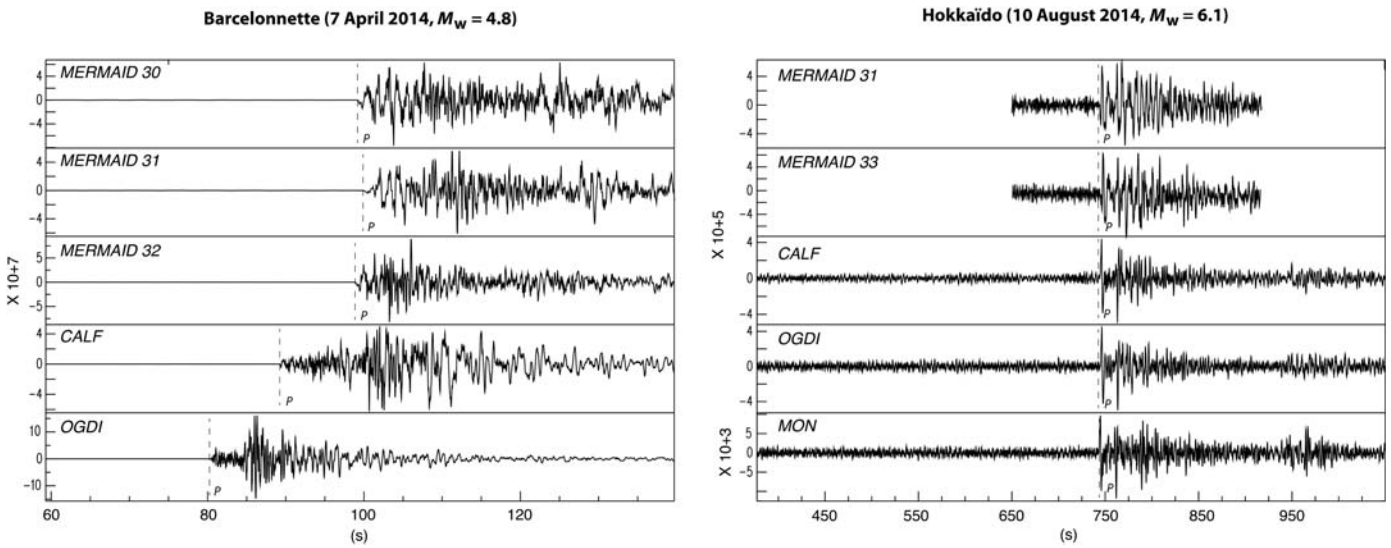

▲ **Figure 6.** Regional Barcelonnette (France, 7 April 2014, M_w 4.8) and teleseimic Hokkaïdo (Japan, 10 August 2014 M_w 6.1) earthquakes recorded by MERMAID floats and terrestrial permanent stations. The locations of stations are illustrated in Figure 1. The time axis is in seconds and begins at 19:25:45 for the Barcelonnette earthquake and at 03:43:20 for the Hokkaïdo earthquake. The amplitude axis is in counts.

French and Italian permanent stations represent 86% of data and the GROSMARIN campaign represents 11%. We selected 30 MERMAID picks for which the onset picked showed no ambiguity at all for validation.

Resolution Tests

To estimate data errors from the misfit that remains after a tomographic inversion, it is important not to underparametrize the model. For example, if the Earth has anomalies smaller than the voxel size, the tomographic inversion would not be able to fit observed data if these are without error. We therefore first estimated the resolution. We performed checkerboard tests with different anomaly sizes (78 × 78 km, 156 × 156 km, and 234 × 234 km), with ±5% velocity anomalies to test the anomaly size that can be resolved with our dataset (Fig. 8a). If an anomaly size cannot be resolved, data misfits cannot be due to underparameterizing, but must be due to errors in observations. We found that the voxel size of 78 km can nowhere be resolved, but locally an acceptable resolution is obtained for a checkerboard with anomalies of 156 × 156 km, as illustrated in Figure 8. We conclude that our voxel size of 78 km is suitable for error estimation.

We also tested the influence of each dataset on the resolution of the solution: (1) the data of terrestrial French and Italian stations in Figure 8b, (2) terrestrial stations combined with GROSMARIN OBS data (Fig. 8c), and (3) the two previous datasets and the MERMAID data (Fig. 8d).

We generally observe that the amplitude of velocity anomalies is poorly reproduced, we reconstruct around ±1% of the ±5% introduced. Nevertheless, we see a minor resolution improvement from the case with onshore stations (dataset 1, Fig. 8b) to the one including marine stations (dataset 3, Fig. 8d). This improvement of the velocity amplitude reconstitution is mainly localized below the central positive cell in southeast France. An improvement from Figure 8c (data set 2) to Figure 8d (data set 3) is barely perceptible, showing that the land and OBS data dominate the solution and allow for validation of the MERMAID picks. Although, we do not have an overdetermined system to perform a formal cross validation, the resolution test shows us that it would be impossible to fit differences of closely spaced MERMAIDs and OBS or land stations by tweaking the model. *A posteriori* misfits thus give us an impression of the errors in the picked onset times.

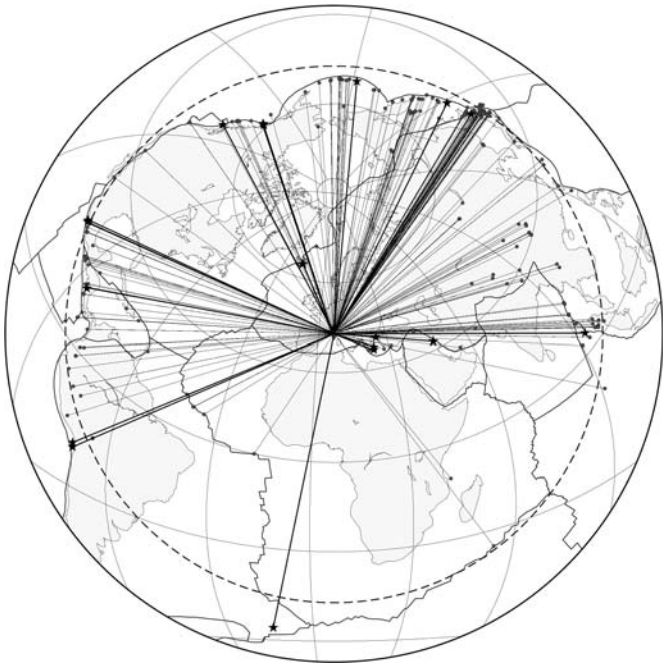

▲ **Figure 7.** Coverage map illustrating the 199 earthquakes used in this study. The dashed circle shows the 90° epicentral distance centered around the study zone.

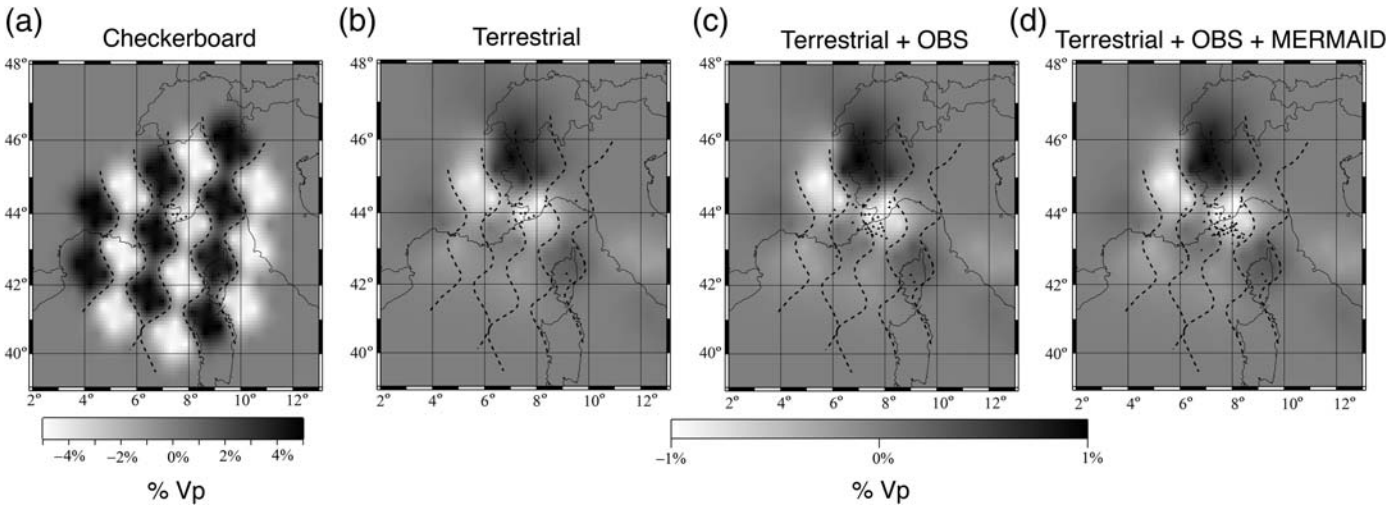

▲ **Figure 8.** Checkerboard resolution tests based on 156 × 156 km anomalies at 226 km depth. (a) The checkerboard used with ±5% velocity anomalies, (b) the solution obtained with data acquired with terrestrial stations only, (c) solution obtained with terrestrial and GROSMARIN OBS stations, and (d) the solution obtained with the two previous datasets and MERMAID floats data. The dotted black curves correspond to the limits between illustrated cells in (a).

Results

We inverted all data simultaneously. The geodynamics of the Ligurian basin are well constrained by various previous tomographic studies. We visually checked that our solution was consistent with the tomographic results from Piromallo and Morelli (2003) and Spakman and Wortel (2004). We damp the inversion so as to obtain a χ^2 that is compatible with the prior error estimate of 0.4 s. The root mean square posterior misfit for all data is 0.43 s. The distribution of the misfits for the MERMAID picks only does not follow a typical Gaussian distribution, but we find that 67% of MERMAID data have a misfit between ±0.17 s. Six potential outliers have a misfit higher than 0.5 s. Figure 9 illustrates the misfit observed at each MERMAID float position.

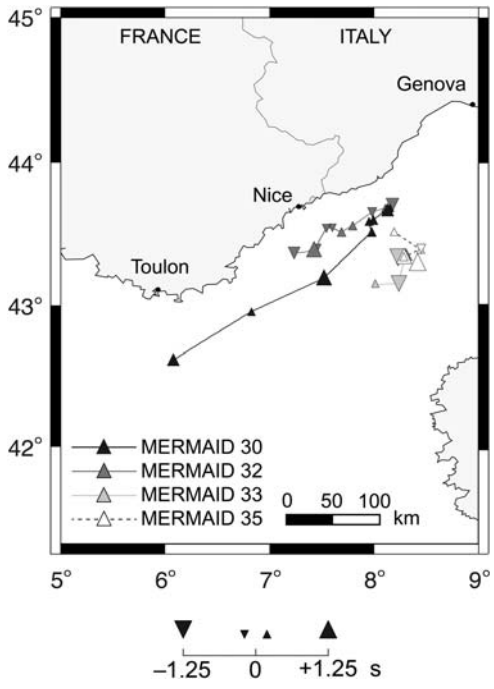

▲ **Figure 9.** Misfits observed at the MERMAID floats positions. Triangles illustrate the misfit, proportional to the observed value. Triangles and reverse triangles indicate positive and negative values of the misfit, respectively.

CONCLUSIONS

In this study, we developed a method to determine float locations by interpolation and extrapolation, and we estimate errors in picks from MERMAID seismograms by incorporating them with other data in a tomographic inversion for the structure beneath the Ligurian basin.

Two disadvantages are that the MERMAID speed depends on the current and their trajectories cannot be controlled. Repeated measurements of delays from the same earthquake region are therefore impossible because the MERMAID changes position. There is thus no simple reduction of errors by averaging. However, averaging is not the only way to reduce errors. Because deep drift is slow (in our experiment it was ∼1.8 km/day, measured from the black trajectories shown inn Fig. 2), aftershock ray paths will still be close, and such data are not independent. A linear inversion will then reduce error by performing a regression by least squares.

After the inversion procedure, we obtain the promising result that 67% of MERMAID data have a misfit between ±0.17 s (Fig. 9). The presence of outliers (20% > 0.50 s) points to the need to develop more sophistical techniques for correcting the delays. In addition, automated techniques for more reliably determining onset times than is possible by eye if the seismogram is noisy could significantly raise the fraction of useful data. We conclude that without sophisticated filters, we can read onset times with precision comparable to that of land stations.

A big advantage of the floating seismometers is that, with an investment of about $20,000 per float, MERMAIDs offer the opportunity to cover large water-covered domains at relatively low cost.

DATA AND RESOURCES

Data acquired in the Ligurian basin and Indian Ocean with MERMAID floats are available at https://www.geoazur.fr/GLOBALSEIS/Data.html (last accessed November 2015). Data are available about one week after data transmission.

ACKNOWLEDGMENTS

We thank Haiying Gao, two anonymous reviewers, and the Editor-in-Chief Zhigang Peng for their fruitful comments that helped improve the manuscript. We also thank Mickaël Bonnin, Jenny Trevisan, Inna Slezak, and Christophe Maron for their help, especially Jenny Trevisan for Figures 2–4. We also thank Sébastien Migeon for the access to data from the MArge LIgure par utilisation du Système Acoustique Remorqué campaign. Some parts of the figures were produced with Generic Mapping Tool (GMT) software (Wessel and Smith, 1991; Wessel *et al.*, 2013). This work is supported by the European Research Council (Advanced Grant 226837).

REFERENCES

Bassin, C., G. Laske, and G. Masters (2000). The current limits of resolution for surface wave tomography in North America, *Eos Trans. AGU* **81,** F897.

Béthoux, J.-P., L. Prieur, and J.-H. Bong (1988). Le courant Ligure au large de Nice, *Oceanol. Acta* 59–67 (in French).

Bézier, P. (1977). Essai de définition des courbes et surfaces expérimentales: Contribution à l'étude des propriétés des courbes et des surfaces paramétriques polynomiales à coefficient vectoriels, *Ph.D. Thesis*, Université Pierre et Marie Curie, Paris, France (in French).

Bézier, P. (1987). *Courbes et surfaces pour la CFAO*, Techniques Ingénieur Ed., Saint-Denis, France, 1–15 (in French).

Bonnin, M., G. Nolet, A. Villasenor, J. Gallart, and C. Thomas (2014). Multiple-frequency tomography of the upper mantle beneath the African/Iberian collision zone, *Geophys. J. Int.* **198,** 1458–1473, doi: 10.1093/gji/ggu214.

Charléty, J., S. Voronin, G. Nolet, I. Loris, F. J. Simons, K. Sigloch, and I. C. Daubechies (2013). Global seismic tomography with sparsity constraints: Comparison with smoothing and damping regularization, *Geophys. Res. Lett.* **118,** 1–13.

Dalton, R. (2002). Oceanography: Voyage of the argonauts, *Nature* **415,** 954–955.

Dessa, J.-X., S. Simons, M. Lelievre, M.-O. Beslier, A. Deschamps, N. Béthoux, S. Solarino, F. Sage, E. Eva, G. Ferretti, O. Bellier, and C. Eva (2011). The GROSMARIN experiment: Three-dimensional crustal structure of the north Ligurian margin from refraction tomography and preliminary analysis of microseismic measurements, *Bulletin de la Société Géologique de France* **182,** 305–321.

Gao, H., and S. Schwartz (2015). Preface to the focus section on Cascadia Initiative preliminary results, *Seismol. Res. Lett.* **86,** no. 5, doi: 10.1785/0220150160.

Gould, J. (2004). Argo profiling floats bring new era of in situ ocean observations, *Eos Trans. AGU* **85,** 185–191.

Hello, Y., A. Ogé, A. Sukhovich, and G. Nolet (2011). Modern mermaid: New floats image the deep Earth, *Eos Trans. AGU* **92,** 337–338.

Kennett, B. L. N., and E. R. Engdahl (1991). Traveltimes for global earthquake location and phase identification, *Geophys. J. Int.* **105,** 429–465.

Migeon, S., A. Cattaneo, V. Hassoun, C. Larroque, N. Corradi, F. Fanucci, A. Dano, B. Mercier de Lepinay, F. Sage, and C. Gorini (2011). Morphology, distribution and origin of recent submarine landslides of the Ligurian margin (North-western Mediterranean): Some insights into geohazard assessment, *Marine Geophys. Res.* **32,** 225–243.

Piromallo, C., and A. Morelli (2003). *P* wave tomography of the mantle under the Alpine-Mediterranean area, *Geophys. Res. Lett.* **108,** no. B2, 2065.

Simons, F. J., I. Loris, G. Nolet, I. C. Daubechies, S. Voronin, J. S. Judd, P. A. Vetter, J. Charléty, and C. Vonesch (2011). Solving or resolving global tomographic models with spherical wavelets, and the scale and sparsity of seismic heterogeneity, *Geophys. J. Int.* **187,** 969–969.

Simons, F. J., G. Nolet, J. M. Babcock, R. E. Davis, and J. A. Orcutt (2006). A future for drifting seismic networks, *Eos Trans. AGU* **87,** 305–307.

Spakman, W., and M. J. R. Wortel (2004). Tomographic view on western Mediterranean geodynamics, in *The TRANSMED Atlas, The Mediterranean Region from Crust to Mantle*, Springer, Berlin, Germany, 31–52.

Sukhovich, A., S. Bonnieux, Y. Hello, J.-O. Irisson, F.-J. Simons, and G. Nolet (2015). Seismic monitoring in the oceans by autonomous floats, *Nat. Comm.* **6,** 8027-1–8027-5, doi: 10.1038/ncomms9027.

Sukhovich, A., J.-O. Irisson, F. J. Simons, A. Ogé, Y. Hello, A. Deschamps, and G. Nolet (2011). Automatic discrimination of underwater acoustic signals generated by teleseismic *P* waves: A probabilistic approach, *Geophys. Res. Lett.* **38,** L18605, doi: 10.1029/2011gl048474.

Wessel, P., and W. H. F. Smith (1991). Free software helps map and display data, *Eos Trans. AGU* **72,** 441–446.

Wessel, P., W. H. F. Smith, R. Scharroo, J. Luis, and F. Wobbe (2013). Generic Mapping Tools: Improved version released, *Eos Trans. AGU* **94,** 409–410.

Cécile Joubert[1]
Guust Nolet
Sébastien Bonnieux
Anne Deschamps
Yann Hello
Université Nice-Sophia Antipolis
Centre National de la Recherche Scientifique
Institut de Recherche pour le Développement
Observatoire de la Côte d'Azur
Géoazur Unité Mixte de Recherche 7329
250 rue Albert Einstein
Sophia Antipolis 06560 Valbonne
France
c.joubert@unistra.fr

Jean-Xavier Dessa
Université Pierre et Marie Curie
Géoazur
CNRS, IRD
Observatoire de la Côte d'Azur
UMR 7329
250 rue Albert Einstein
Sophia Antipolis 06560 Valbonne
France

Published Online 16 December 2015

[1] Now at Institut de Physique du Globe de Strasbourg, Unité Mixte de Recherche 7516, Université de Strasbourg/EOST, Centre National de la Recherche Scientifique, 5 rue René Descartes, F-67084 Strasbourg Cedex, France.